Effect of spatial defect distribution on the electrical behavior of prominent vacancy point defects in swift-ion implanted Si

L. Vines,[1,*] E. V. Monakhov,[1] J. Jensen,[2] A. Yu. Kuznetsov,[1] and B. G. Svensson[1]
[1]*Department of Physics/Physical Electronics, University of Oslo, P.O. Box 1048 Blindern, N-0316 Oslo, Norway*
[2]*Division of Ion Physics, Uppsala University, Box 534, SE-751 21 Uppsala, Sweden*
(Received 4 February 2008; published 19 February 2009)

Samples of epitaxially grown *n*-type silicon have been implanted at room temperature with low doses (10^6–10^9 cm^{-2}) of He, C, Si, and I ions using energies from 2.75 to 46 MeV. Deep level transient spectroscopy studies reveal that the generation of divacancy (V_2) and vacancy-oxygen (VO) pairs has a distinct ion mass dependence. Especially, the doubly negative charge state of the divacancy, $V_2(=/-)$, decreases in intensity with increasing ion mass compared to that of the singly negative charge state of the divacancy, $V_2(-/0)$. In addition, the measurements show also a decrease in the intensity of the level assigned to VO compared to that of $V_2(-/0)$ with increasing ion mass. Carrier capture cross-section measurements demonstrate a reduction in the electron capture rate with increasing ion mass for all the three levels $V_2(-/0)$, $V_2(=/-)$, and VO; but a gradual recovery occurs with annealing. Concurrently, the strength of the $V_2(-/0)$ level decreases in a wide temperature range starting from below 200 °C, accompanied by an increase in the amplitudes of both the VO and $V_2(=/-)$ peaks. In order to account for these results a model is introduced where local carrier compensation is a key feature and where two modes of V_2 are considered: (1) V_2 centers located in regions with a high defect density around the ion track (V_2^{dense}) and (2) V_2 centers located in regions with a low defect density (V_2^{dilute}). The V_2^{dense} fraction does not give any contribution to the $V_2(=/-)$ signal due to local carrier compensation, and the amplitude of the $V_2(=/-)$ level is determined by the V_2^{dilute} fraction only. The spatial distributions of defects generated by single-ion impacts were simulated by Monte Carlo calculations in the binary collision approximation, and to distinguish between the regions with V_2^{dense} and V_2^{dilute} a threshold for the defect generation rate was introduced. The model is shown to give good quantitative agreement with the experimentally observed ion mass dependence for the ratio between the amplitudes of the $V_2(=/-)$ and $V_2(-/0)$ peaks. In particular, the threshold value for the defect generation rate remains constant (~1.2 vacancies/ion/Å) irrespective of the type of ion used, which provides strong evidence for the validity of the model. Annealing at temperatures above ~300 °C is found to reduce the spatial localization of the defects and migration of V_2 occurs with subsequent trapping by interstitial oxygen atoms and formation of divacancy-oxygen pairs.

DOI: 10.1103/PhysRevB.79.075206 PACS number(s): 71.55.Cn, 61.72.Bb, 61.72.jd

I. INTRODUCTION

Vacancy-related defects, e.g., vacancy-oxygen (VO) pairs and divacancy centers (V_2), are fundamental electrically active point defects generated in silicon by ion implantation. It is well established that VO is associated with an acceptor level at $E_c-0.18$ eV,[1] while V_2 provides two electronic states in the upper part of the band gap, located at $E_c-0.23$ and $E_c-0.43$ eV and associated with doubly $[V_2(=/-)]$ and singly $[V_2(-/0)]$ negatively charged divacancies,[2,3] respectively, (E_c denotes the conduction band edge). Interestingly, when monitoring the divacancy in electron-irradiated and heavy ion implanted *n*-type samples by deep level transient spectroscopy (DLTS), the relative intensity of the two divacancy signals exhibits a quite different behavior.[4,5] In electron-irradiated samples, a close one-to-one proportionality holds between the DLTS amplitudes of the $V_2(=/-)$ and $V_2(-/0)$ states,[6,7] while in heavy ion implanted samples, the $V_2(=/-)$ intensity is strongly reduced compared to that of $V_2(-/0)$.[8] A similar effect is also observed in neutron irradiated samples.[9,10] The reduction increases with ion mass, referred to in literature as the ion mass effect, and has been reported in materials with *n*-type doping from 3×10^{13} to 1.6×10^{16} cm^{-3}.[5,8,11,12]

At least three different models/reasons have been proposed to explain this behavior: (i) lattice strain induced by heavy ion collision cascades prevents motional averaging of V_2 at low temperatures favoring $V_2(-/0)$ over $V_2(=/-)$ (Refs. 5 and 8); (ii) additional electrically active defects, e.g., large vacancy clusters ($V_x, x>2$), contribute to the DLTS peak at $E_c-0.43$ eV artificially enhancing the "$V_2(-/0)$" signal;[13] and (iii) incomplete occupation of the $V_2(=/-)$ state occurs due to local carrier compensation around the ion trajectory.[12,14] Models (i) and (iii) are consistent with several associated experimental observations. First, they explain the reduction in the carrier capture rate of $V_2(=/-)$ with increasing ion mass.[12] Second, the reduced difference in peak amplitude between the $V_2(=/-)$ and $V_2(-/0)$ states when implanting at elevated temperatures is accounted for.[8] Third, in particular model (iii) predicts the occurrence of a charge distribution pattern formed by single-ion impacts as observed by scanning capacitance microscopy.[15] Furthermore, model (iii) has a distinct advantage since it can be employed for quantitative estimates, and simulations have also confirmed that incomplete occupation of $V_2(=/-)$ (and VO) can indeed occur in locally compensated samples if the defect concentration is sufficiently high.[12] However, there is still no consensus on the origin of the ion mass effect, and more studies are needed both to verify the proposed mechanisms and to improve the understanding of vacancy clustering in Si after heavy ion implantation. In particular, the annealing behavior

in the compensated defect regions is not well documented for impurity- (C, O, H, etc.) lean material and can reveal additional arguments supporting or excluding mechanisms (i)–(iii). For example, it is known from studies of electron-irradiated high purity Si that V_2 is stable in a rather wide temperature range and has a diffusion coefficient of $\sim 3 \times 10^{-3}[\mathrm{cm}^2/\mathrm{s}]\exp-\frac{1.3[\mathrm{eV}]}{k_B T}$,[16] where k_B is Boltzmann's constant and T is the absolute temperature; in such materials V_2 anneals out predominantly through migration and subsequent trapping by interstitial oxygen atoms, forming a divacancy-oxygen center (V_2O).[16–19] Thus, heat treatment at 200–300 °C may result in a significant diffusion of V_2 within the highly damaged regions, where the V_2's are closely located, likely reducing the local compensation effect as well as reducing the strain preventing motional averaging of V_2.

Combining results from simulations of (a) the defect distributions induced by single-ion impacts and (b) the charge-carrier population in defect-rich regions, evidence is obtained that local compensation arises mainly in regions damaged by energetic recoils (and their associated collision cascades). In such regions, the concentration of V_2 centers can be sufficiently high to cause pinning of the Fermi level at the $V_2(-/0)$ state. Hence, a principal distinction can be made between two divacancy components—V_2^{dilute} and V_2^{dense}. The former one occurs in less-damaged regions with a sufficient amount of electrons available to occupy the $V_2(=/-)$ state. The latter one is confined to the ion /recoil track regions where the occupancy of $V_2(=/-)$ is close to zero. In accordance with the experiments, the simulations indicate also an incomplete occupancy of the VO state despite the fact that the VO centers are expected to have a wider spatial distribution than the V_2 centers. Furthermore, quantitative modeling of the ion mass effect for the $V_2(=/-)$ and $V_2(-/0)$ states is undertaken and displays good agreement with experimental data provided that a spatial distribution of sufficient accuracy is used for the V_2 centers. Results from annealing studies and filling pulse measurements of the defect states are discussed qualitatively, and they favor strongly the local compensation model.

II. EXPERIMENTAL

$p^+n^-n^+$ diodes were fabricated from an epitaxial silicon structure grown by chemical vapor deposition (CVD) having a carrier concentration of 1×10^{14} cm^{-3} in the n^- region. Front and backside Ohmic contacts to the p^+ and n^+ regions were made by Al evaporation. The thickness of the epi-n^- layer was ~ 60 μm. Chemical profiling using secondary-ion-mass spectrometry revealed carbon and oxygen concentrations in the epilayers of below 5×10^{16} and 2×10^{17} cm^{-3}, respectively. The fully processed samples were then implanted at room temperature (RT) at the Tandem Laboratory, Uppsala University, with He, C, Si, and I ions at energies of 2.75, 11, 30, and 46 MeV, respectively, and with doses from 6×10^6 to 2×10^8 cm^{-2}. The energies have been selected to give approximately the same projected range at about 10 μm.

DLTS and minority carrier transient spectroscopy (MCTS) were carried out using a refined version of a setup described in detail elsewhere.[20] In short, the sample temperature was scanned between 77 and 300 K, where the capacitance transients were averaged within an interval of 1 K. The DLTS signal was extracted using a lock-in type of weighting function with six traditional rate windows from (20 ms)$^{-1}$ to (640 ms)$^{-1}$, applying a reverse bias of typically −10 V and a filling pulse of +10 V with 50 ms duration. During the MCTS measurements the filling pulse amplitude was +13 V resulting in a sufficient hole injection to fill minority carrier traps. The isochronal annealing was performed in 25 °C steps (20 min) and ranging from 150 to 400 °C.

Monte Carlo simulations were performed by TRIM (Ref. 21) and used for estimating the total vacancy generation by the different ions studied experimentally. These data were also used as input when calculating the occupancy of the VO and V_2 states assuming 1% of the generated vacancies to form V_2's in accordance with the results in Ref 8.

Calculations of the trap occupancy were performed by charge-carrier simulations using the commercially available Synopsys Sentaurus technology computer aided design (TCAD) software.[22] The calculations have been made within the drift-diffusion transport approximation, accounting for incomplete ionization and applying a circular symmetry for the ion track structure. The track structure assumed consists of a narrow defect-rich region surrounded by a defect free matrix. The defect region is simulated as containing two defect levels having the characteristics of $V_2(-/0)$ and $V_2(=/-)$. The energy levels of $V_2(-/0)$ and $V_2(=/-)$ were put to $E_c-0.43$ and $E_c-0.23$ eV, respectively, while the electron and hole capture cross sections used were 5×10^{-15} and 5×10^{-14} cm^2 for $V_2(-/0)$, respectively, and 2×10^{-15} and 1.4×10^{-12} cm^2 for $V_2(=/-)$, respectively.[12,23] In these simulations the VO center was omitted since the energy position of its acceptor state is shallower than both the V_2 states. Further, because the formation process of VO involves substantial migration of monovacancies and trapping by oxygen interstitials (O_i), the VO centers are expected to be more widely distributed in space than V_2, with only a minor influence on the $V_2(=/-)$ occupancy.

III. RESULTS

A. Simulations of defect formation

Figure 1(a) shows the results of the TRIM simulation of a single I impact (46 MeV) into Si, using a threshold displacement energy of $T_d=15$ eV. The generated vacancies occur both along the ion trajectory as well as in the subsequent collision cascades and are primarily generated within a narrow region ($\lesssim$20 nm), around the ion/recoil trajectories. In Fig. 1(b), the vacancy generation per ion and angstrom versus depth after a single I impact is illustrated, while Fig. 1(c) shows the average after 400 I impacts. It is clearly seen that the regions having the highest vacancy generation rate after a single-ion impact [defined by the dashed line in Fig. 1(b)] are not revealed after statistical (arithmetic) averaging over a large number of impacts [Fig. 1(c)].

It is known that stable defect complexes can form both during the initial Frenkel pair generation and during the subsequent migration of vacancies and interstitials. Specifically,

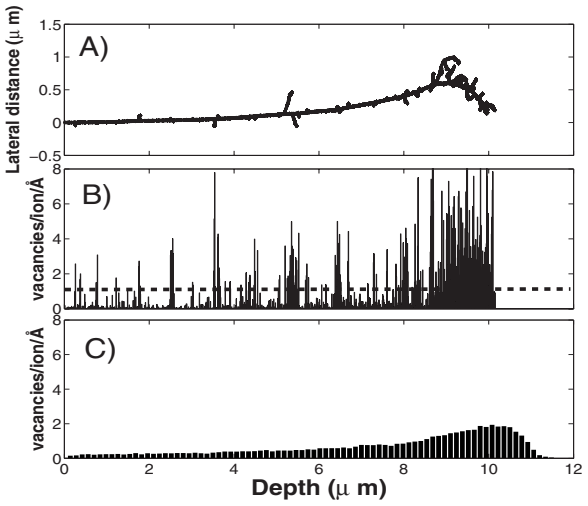

FIG. 1. TRIM simulation of a 46 MeV I impact in Si, showing (a) the lateral and depth distribution of generated vacancies, (b) the generated vacancies from a typical single impact, and (c) the average vacancy generation after simulation of 400 impacts. The dashed line in (b) indicates a threshold level for reduced occupancy of the $V_2(=/-)$ state to occur, and will be discussed in Sec. IV.

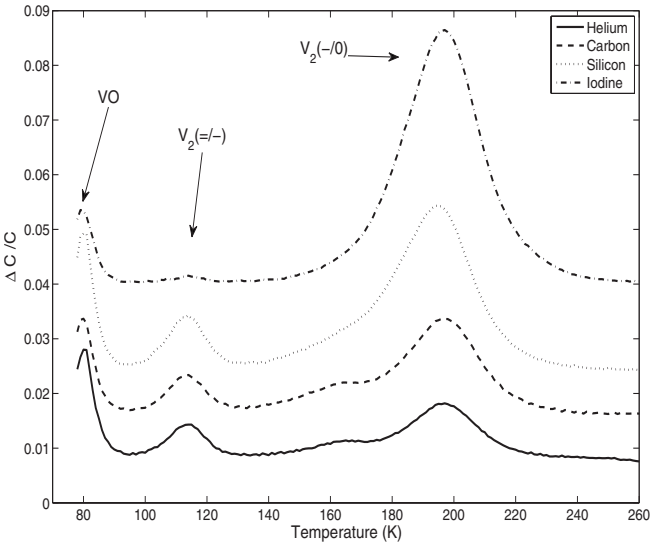

FIG. 2. DLTS spectra of epi-Si after implantation with different ions. Offsets have been applied to separate the lines for clarity. $\Delta C/C$ is the DLTS signal (ΔC) divided by the reverse bias capacitance (C).

divacancies in Si are known to form both by pairing of two migrating monovacancies originating from the same impact[24] and directly when two nearest-neighbor Si atoms are displaced by the impinging ion or recoiling atoms.[2]

In order to displace two nearest-neighbor atoms, the energy deposition must be considerably larger than for generating a monovacancy. For example, assuming the displacement energy for direct divacancy formation to be 70 eV, TRIM simulations of a 46 MeV I impact with T_d=70 eV show similar features as in Fig. 1, both for the individual track [Figs. 1(a) and 1(b)] and for the average over 400 tracks [Fig. 1(c)], but the amount of the generated defects is only 15%–25% of that for T_d=15 eV. However, this is still one order of magnitude above the experimentally observed V_2 generation, indicating that a major fraction of the V_2's is generated directly, even if the reaction $V_2+I\rightarrow V$ is taken into account. Divacancies generated at this initial collisional stage are likely to form with a high density in spatial regions along the ion/recoil trajectories, as illustrated in Fig. 1(a), and these regions correspond to the spikes in the defect generation rate [Fig. 1(b)]. In contrast, divacancies generated by pairing through vacancy migration will potentially have a larger separation in space.

In this context, it should be emphasized that there are alternative ways of describing the defect evolution after heavy ion impact than the binary collision approximation in random phase targets assumed by TRIM. Especially, molecular dynamics (MD) simulations have proven to be very useful in understanding the initial defect evolution ($\lesssim 10^{-10}$ s) in crystalline Si bombarded with low energy ($\lesssim$10 keV) ions.[25–27] In accordance with experimental results, very few isolated Frenkel pairs of V's and I's are found to be produced by single-collision cascades; i.e., spontaneous annihilation is strong already at an early stage long before the so-called diffusion stage of a cascade development. However, the MD simulations also predict that large defect clusters, or even pockets of unrelaxed disordered material, can be formed by the collision cascades. These disordered regions are surrounded by crystalline material and rather rapid recrystallization may be anticipated, relative to that of a planar amorphous-crystal interface. Our electrical measurements, using DLTS and MCTS, do not reveal any pronounced band-gap states to be associated with these defect-rich regions (clusters), but they are likely to affect the charge-carrier population of electrically active point defects located in the vicinity of these regions, as will be further discussed later for the V_2 and VO centers.

B. Transient capacitance spectroscopy measurements

Figure 2 shows DLTS spectra with three dominant defect levels after He, C, Si, and I implantations. The levels are well established in the literature[6,7,28] and assigned to VO, $V_2(-/0)$, and $V_2(=/-)$, respectively. The amplitudes of both the VO and $V_2(=/-)$ signals are reduced with increasing ion mass as compared to that of $V_2(-/0)$.

On the basis of the rate of elastic energy deposition and as illustrated in Fig. 1, local compensation and lattice distortion should be most pronounced at the depth of the ion range, as compared to the tail region where the collisions result in much lower defect density [Fig. 1(b)]. Indeed, Fig. 3 demonstrates a decrease in the amplitude of both the $V_2(=/-)$ and VO signals versus the $V_2(-/0)$ intensity in the end-of-range region, and the two V_2 signals display a close one-to-one relation in the tail region.

Figure 4 shows results of isochronal heat treatments for 20 min in the range of 150–400 °C. At sufficiently high temperatures, V_2 starts to transform into V_2O and the contributions from these two complexes, which have closely spaced energy levels for both the singly and doubly negative charge states,[16–19] have been separated by fitting of the ex-

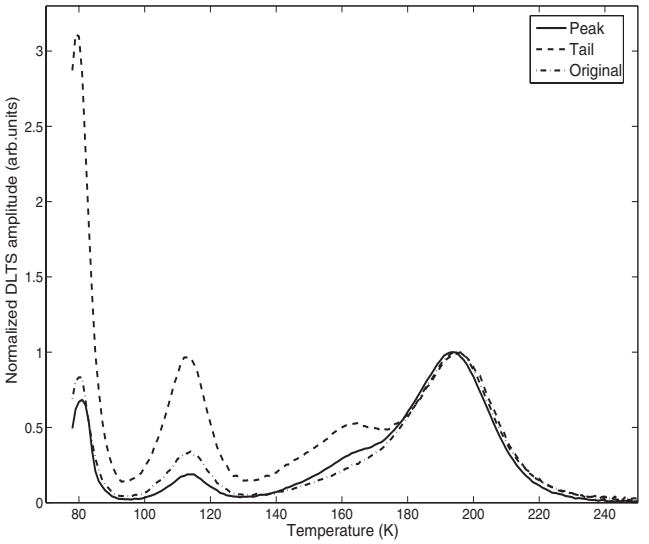

FIG. 3. DLTS spectra of Si implanted with 30 MeV Si, where the filling pulse height and bias have been chosen to probe the tail (depth of 4–7 μm) and peak (depth of 7–10 μm) of the defect distribution, and the entire profile of the defects (depth of 0–12 μm). The DLTS amplitudes have been normalized with respect to the $V_2(-/0)$ peak.

perimental DLTS data assuming that V_2 only is present for annealing temperatures $\leq$225 °C and V_2O only above 350 °C. In all the samples, the amplitude of $V_2(-/0)$ starts to decrease gradually above 150 °C and is below the detection limit after ~325 °C. The amplitude of the $V_2(=/-)$ peak is stable or even increases up to ~250 °C (Fig. 4) before decreasing to the detection limit at ~325 °C. The fact that the $V_2(-/0)$ signal decreases over a wide temperature range while $V_2(=/-)$ exhibits a reverse annealing behavior, i.e., the signal strength increases during annealing, indicates that V_2 experiences a complex annealing kinetics. The annealing of V_2 is correlated with the rise of V_2O, and the two levels attributed to V_2O$(=/-)$ and V_2O$(-/0)$, respectively, increase in amplitude from ~275 to 325 °C, before annealing out around 350–375 °C.[16,29,30]

Interestingly, the signal of VO displays a similar increasing trend as that of $V_2(=/-)$ in the Si- and I-implanted samples and the trend persists up to ~300 °C. Above 350 °C, the VO signal starts to decrease rapidly and is below the detection limit after annealing at 400 °C. In this context, it should be mentioned that several secondary defect signatures with small amplitudes arise during the final stages of the heat treatment (above 325 °C). However, they are considered to be of minor importance for the core of this work

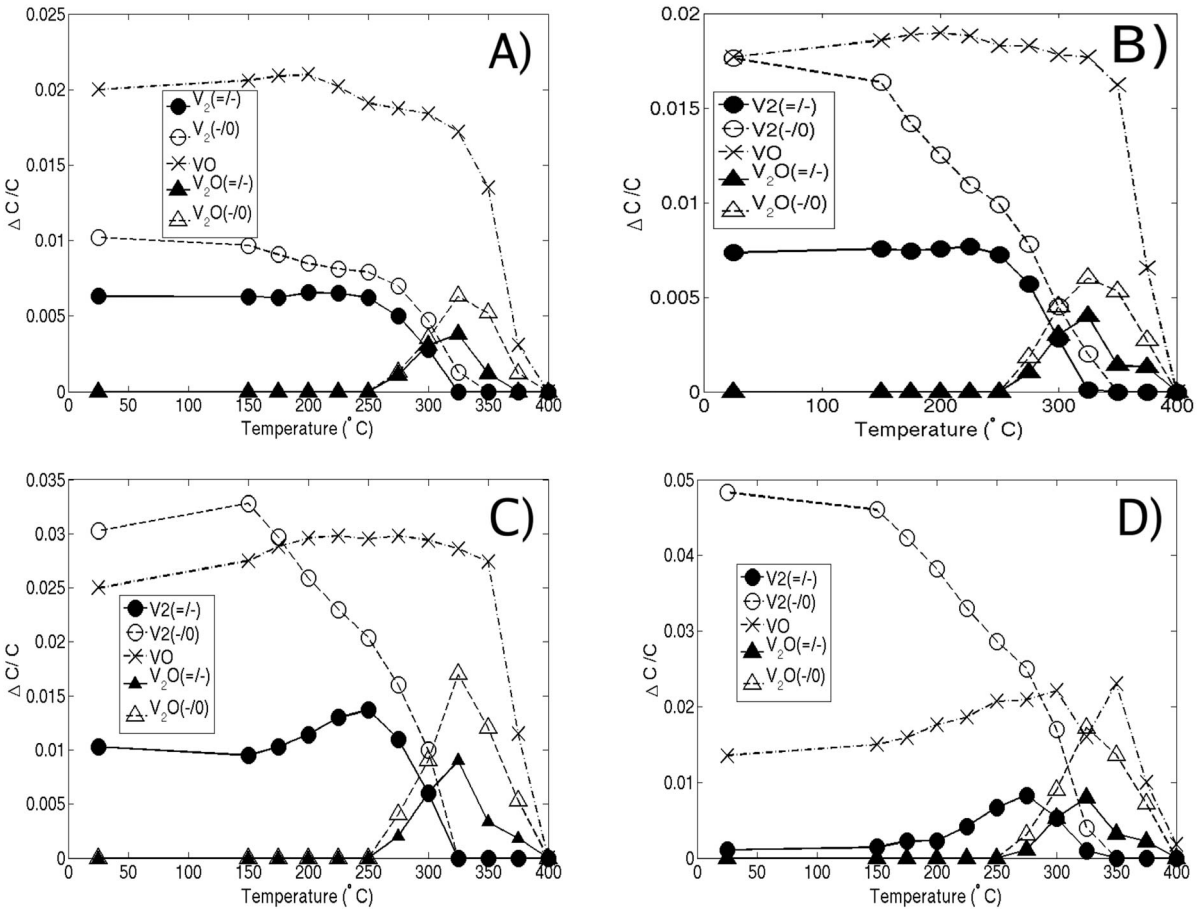

FIG. 4. Peak DLTS amplitude of defect levels in epi-Si irradiated with (a) He, (b) C, (c) Si, and (d) I. $\Delta C/C$ is the DLTS signal (ΔC) divided by the reverse bias capacitance (C).

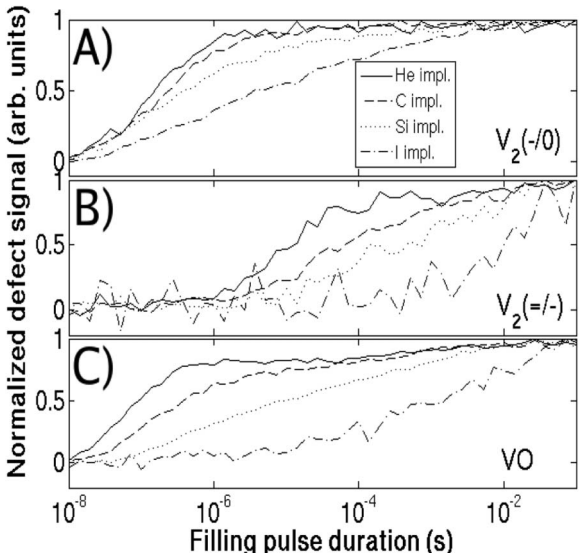

FIG. 5. Filling pulse measurements for the as-implanted samples. Diagrams (a), (b), and (c) correspond to the filling of the $V_2(-/0)$, $V_2(=/-)$, and VO levels, respectively.

and are, therefore, not discussed further. Moreover, MCTS measurements have not revealed formation of any centers correlated with the annealing of the $V_2(-/0)$, $V_2(=/-)$, and VO levels.

Results from filling pulse measurements for the samples studied are shown in Figs. 5 and 6. First, the filling time increases with increasing ion mass for all the three levels [$V_2(-/0)$, $V_2(=/-)$, and VO] (Fig. 5). Interestingly, except for the He implanted samples $V_2(=/-)$ does not reach a saturation level, and a similar observation has been interpreted as incomplete filling due to local compensation.[12] The filling is expected to start for pulse widths $>10^{-6}$ s in the samples used (doping concentration $N_d \sim 10^{14}$ cm^{-3}), according to results from electron-irradiated samples.[14] Figure 6 shows the evolution of the filling time in the Si implanted samples after selected annealing steps. The filling time of both the $V_2(-/0)$ and VO levels clearly decrease with increasing annealing temperature [Figs. 6(a) and 6(c)], while the effect for $V_2(=/-)$ is less pronounced. However, results for I-implanted samples with a higher doping concentration ($\sim 10^{15}$ cm^{-3}) than used in our study (and hence less affected by compensation) show that a decrease in the $V_2(=/-)$ filling time occurs after annealing above ~ 150 °C.[14] On the basis of the data in Figs. 5 and 6 one can unambiguously rule out model (ii), discussed in Sec. I, as the only explanation for the ion mass effect; i.e., the difference in amplitude between the $E_c-0.23$ and $E_c-0.43$ eV levels is not just caused by an additional contribution to the latter one.

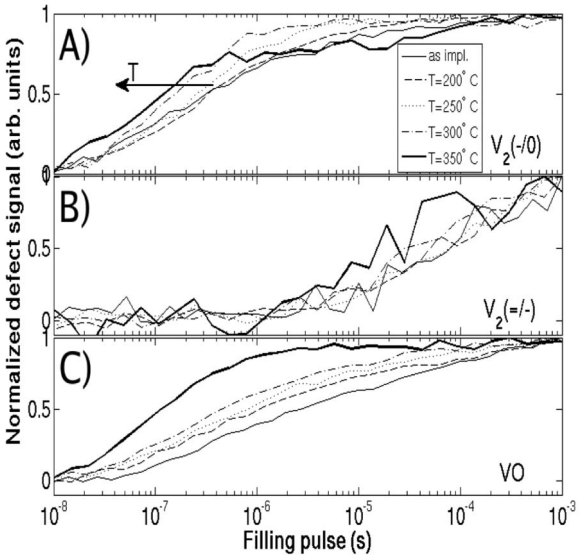

FIG. 6. Filling pulse measurements of the sample implanted with Si ions and subsequently annealed at 200–350 °C. Diagrams (a), (b), and (c) correspond to the filling of the $V_2(-/0)$, $V_2(=/-)$, and VO levels, respectively.

IV. DISCUSSION

In this section, the experimental observations of the V_2, VO, and V_2O centers are discussed within the framework of the local compensation model. Comparison is made with results from TCAD simulations of charge-carrier population of the V_2 acceptor states and with results from Monte Carlo simulations of the spatial defect distribution. Especially, it is found to be of crucial importance that the effects of individual ion tracks are considered and interpretations based on average defect distributions do not apply.

A. Charge-carrier population of the $V_2(-/0)$ and $V_2(=/-)$ states and the influence by ion mass

As a first approximation, one can estimate the average defect concentration around an ion trajectory assuming that the defects form a continuous channel.[12] For instance, the average peak generation rate of vacancies after a 46 MeV I impact is 1.9/ion/Å, according to results from TRIM simulations [Fig. 1(c)]. The projected range is approximately 10 μm, resulting in $\leq 2.0 \times 10^5$ vacancies around each ion trajectory. In addition, one should account for the fact that vacancy-interstitial recombination is strong and only about 1% of the initially generated vacancies survive to form V_2.[8] Hence, the resulting average density of V_2 centers in a defect region of cylindrical shape along the ion track and with a radius of 15 nm (Fig. 1) becomes roughly 3×10^{17} cm^{-3}.

Using this estimation for the V_2 density, results from TCAD steady-state simulations of the occupancy of the $V_2(=/-)$ level are illustrated in Fig. 7 for different vacancy generation rates, corresponding to impacts by ions with different masses and energies in the MeV range. The simulations were performed as a function of the defect region radius, while the total amount of V_2's was kept fixed. Figure 7 shows that the generation rate of 1.9 vacancies/ion/Å; i.e., an I impact, gives rise to a reduced occupancy of the $V_2(=/-)$ level and that the occupancy increases with increasing track radius. In the highly doped material ($N_d = 10^{16}$ cm^{-3}) a complete occupancy occurs for track radii exceeding ~ 30 nm while in the low doped material ($N_d = 10^{14}$ cm^{-3}) a reduced occupancy persists even for a radius of 100 nm. In contrast, using lighter ions, e.g., carbon, a complete occu-

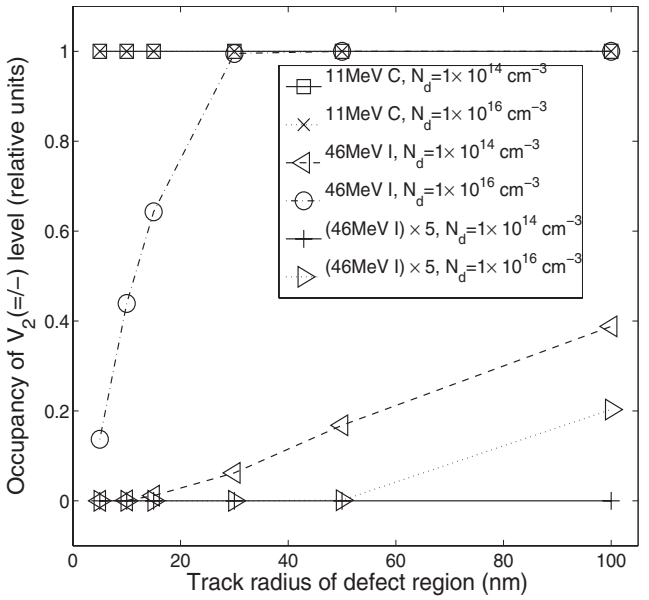

FIG. 7. Simulated occupancy of the $V_2(=/-)$ level versus track radius for different defect concentrations, corresponding to C, I, and $5\times I$ ion irradiations, and for doping concentrations of 1×10^{14} and 1×10^{16} cm^{-3}. N_d is the donor concentration.

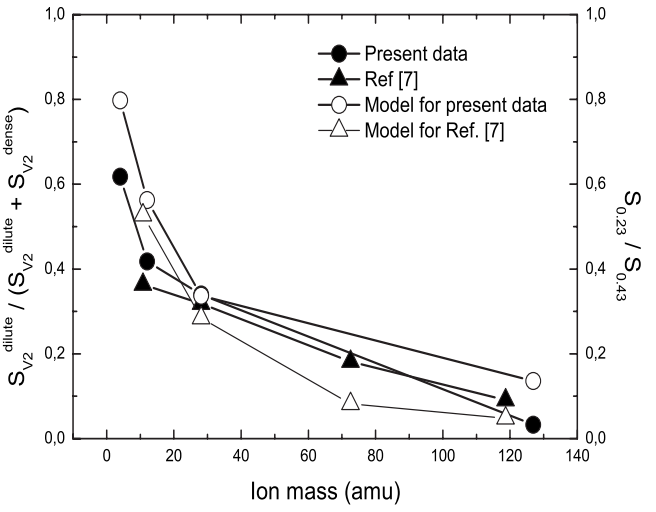

FIG. 8. Fraction of divacancies in the dilute state obtained by simulations as a function of the ion mass. Experimental data for the ratio $S_{0.23}/S_{0.43}$ obtained from room temperature implants are included for comparison, where $S_{0.23}$ and $S_{0.43}$ are the DLTS amplitude of the $V_2(=/-)$ and $V_2(-/0)$ peaks, respectively.

pancy of $V_2(=/-)$ is obtained irrespective of the track radius and doping concentration used, contradictory to that observed experimentally; see, e.g., Fig. 4(b). Thus, as anticipated from MD simulations,[27] the cylindrical model assumed for the V_2 distribution does not hold, at least not for relatively light ions such as carbon. Here, it should be mentioned that the occupancy of the $V_2(=/-)$ level has not necessarily reached steady state during filling in the DLTS measurements, but this effect is most pronounced for heavy ions and less significant for light ions such as carbon; see Fig. 5. It can also be pointed out that the TCAD steady-state simulations yield essentially complete occupancy of the $V_2(-/0)$ state for all the conditions used in Fig. 7, except for the $5\times$I ones where a reduced occupancy occurs for track radii <100 nm when $N_d=10^{14}$ cm^{-3} and <30 nm when $N_d=10^{16}$ cm^{-3}.

Figure 1(b) reveals that the defect distribution after a single-ion impact is highly nonuniform, featuring high defect densities in the collision cascades while in between the cascades the defect density is significantly lower, indicating that important characteristics may be lost by arithmetic averaging over many ions. In addition, MD simulations reveal that these defect–rich regions exhibit a highly distorted crystal structure[27] and, locally, a low effective carrier concentration and mobility can be expected. Accordingly, a more refined model of the spatial distribution of the V_2 centers is required, accounting for the possibility that V_2 centers can exist in regions with different defect densities. As a first stage, the V_2 centers and the defect regions are divided into two categories; (a) V_2 centers located in regions with a high defect density, V_2^{dense}, and (b) V_2 centers located in regions with a low defect density, V_2^{dilute}. Hence, the measured DLTS signal of $V_2(=/-)$ will mainly arise from V_2^{dilute}, while most of the $(=/-)$ states of V_2^{dense} remain unfilled because of local compensation due to electron pinning by the $V_2(-/0)$ state.

In order to distinguish between categories (a) and (b), a threshold defect generation rate is introduced, as exemplified by the dashed line in Fig. 1(b) for a value of 1.2 vacancies/ion/Å. Thus, the regions in Fig. 1(b) with a generation rate above the threshold value give rise to V_2^{dense}, while the regions with a lower generation rate contribute to V_2^{dilute} only. If the model holds, the threshold should be constant irrespective of the nature of the projectile. Indeed, as shown in Fig. 8 good quantitative agreement is obtained between the experimental data for the ratio $S_{0.23}/S_{0.43}$ and the simulated data for $S_{V_2}^{\text{dilute}}/(S_{V_2}^{\text{dilute}}+S_{V_2}^{\text{dense}})$ versus ion mass using a threshold of 1.2 vacancies/ion/Å for all the types of ions (S denotes DLTS peak amplitude). The simulated DLTS peak amplitudes, $S_{V_2}^{\text{dilute}}$ and $S_{V_2}^{\text{dense}}$, are obtained by integrating the regions with V_2^{dilute} and V_2^{dense}, respectively, and weighting them with depth in order to facilitate direct comparison with the experimental S values. Further, the occupation of the $(=/-)$ state of V_2^{dense} is put to zero and that of V_2^{dilute} is put to one. This procedure is performed for more than 30 ion tracks in order to account for the statistical variations of the individual tracks and deduce "steady state" values of the ratio $S_{V_2}^{\text{dilute}}/(S_{V_2}^{\text{dilute}}+S_{V_2}^{\text{dense}})$, as illustrated in Fig. 9. One can observe that the number of tracks necessary for the fractions to reach "steady state" is lower for heavy ions since the number of generated divacancies per track is larger for these ions.

Moreover, the highly distorted regions containing V_2^{dense} occur mainly around the peak of the projected ion range, while V_2^{dilute} is more pronounced in the tail of the defect distribution. For example, for the Si (30 MeV) impacts, the ratio $S_{V_2}^{\text{dilute}}/(S_{V_2}^{\text{dilute}}+S_{V_2}^{\text{dense}})$ becomes 73% and 33% in the tail and peak regions, respectively, consistent with the experimental results in Fig. 3.

Finally, it should be clearly emphasized that this model implies that the observed ion mass and depth dependence of $S_{0.23}/S_{0.43}$ is exclusively related to the single-ion tracks and

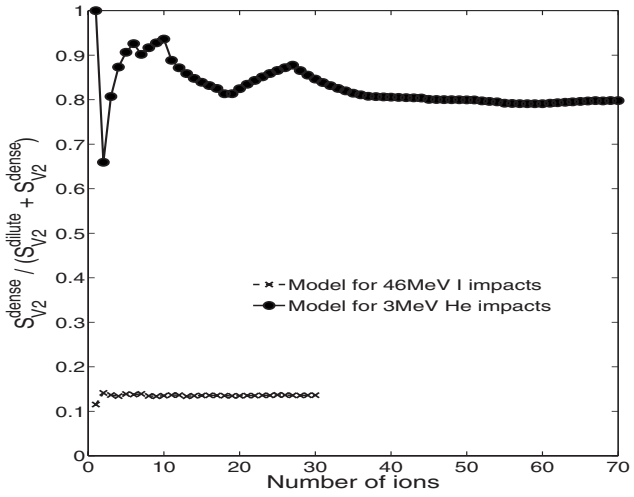

FIG. 9. Fraction of divacancies in the dilute state obtained by simulations as a function of the number of impacts for 3 MeV He and 46 MeV I ion.

their strong spatial localization with respect to the defect generation. It is not possible to reproduce the experimental data in Figs. 3 and 8 by considering arithmetically averaged defect distributions of the kind depicted in Fig. 1(c).

B. Interpretation of the results from the filling pulse measurements using the two-mode divacancy model

The local defect density affects greatly the filling time of a defect level, as seen in Figs. 5 and 6. The filling time is influenced by, e.g., the space charge region around the high density of negatively charged V_2^{dense} centers, and the extension of the space charge can be $0.1-1$ μm depending on the background doping, as shown by the simulation results in Fig. 10. Thus, an increase in filling time applies also for the V_2^{dilute} and VO centers located within the space charge region caused by V_2^{dense}. In fact, this is a major argument in favor of the local compensation model versus the strain model, discussed in Sec. I, since the latter one cannot account for the increased filling time of the VO level. During annealing at temperatures between 200–300 °C the band bending around the space charge region caused by V_2^{dense} is reduced, resulting in a clearly reduced filling time of both the $V_2(-/0)$ and VO states (Fig. 6) and possibly also for $V_2(=/-)$. In the latter case, the conclusion is, however, less obvious because of the low signal-to-noise ratio.

C. Annealing of the V_2 and VO centers and formation of the V_2O pair

As revealed by the data in Fig. 4, the V_2 centers exhibit a complex annealing kinetics. According to the value for the diffusion constant of V_2 given by Mikelsen *et al.*,[16] treatment for 20 min at 200 and 300 °C results in a diffusion length of ~2.3 and ~37 nm, respectively. Thus, above ~200 °C the V_2 diffusion length is comparable with the extension of the defect-rich regions and annealing can occur via agglomeration of V_2^{dense} into larger complexes, $nV_2 \rightarrow V_{2n}$, reducing the $V_2(-/0)$ signal. In addition, the V_2^{dense} fraction can also decrease because of V_2 migration and crystal restoration giving rise to a transition from V_2^{dense} to V_2^{dilute}. Indeed, a rise of 4.1%, 4.2%, and 33% in $S_{0.23}$ is observed for the He, C, and Si implanted samples during annealing, respectively, while in the I-implanted sample $S_{0.23}$ increases by more than eight times relative to the original value (Fig. 4). A similar increasing trend occurs also for the VO peak, where an increase of 5%, 7.3%, and 20% is observed for the He, C, and Si implanted samples, respectively, while for the I-implanted sample the relative increase is a factor of 4. Moreover, it has been shown that local compensation can result in an artificial increase in $S_{0.43}$ by up to ~30%,[12] which will contribute to the decrease in $S_{0.43}$ as the local compensation diminishes during the annealing.

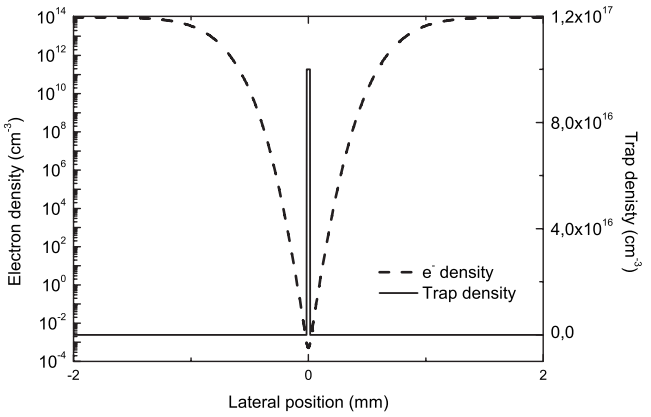

FIG. 10. Electron density as a function of lateral position relative to a cylindrical trajectory with a V_2 density of 1×10^{17} cm^{-3} and a radius of 15 nm. The sample has a uniform background doping concentration of 1×10^{14} cm^{-3}.

Formation of higher order vacancy complexes in regions with a high local V_2 concentration is, indeed, anticipated. For instance, electron paramagnetic resonance (EPR) studies of neutron irradiated samples have revealed signals ascribed to V_4 and V_5 complexes.[31–33] In particular, the V_5 complex is shown to form after annealing at 170 °C and it remains stable until 400 °C. Moreover, calculations based on density-functional theory provide additional support for that several of the V_n complexes are stable up to temperatures in excess of 300 °C.[34] A prime example is the V_6 complex, which in its lowest energy configuration ("missing hexagonal ring") exhibits a binding energy of almost 4 eV relative to V_5 plus V.[35] V_6 is predicted to be electrically (and optically) inactive, and in fact using an experimental concept of platinum in diffusion, Holm and Bonde Nielsen[36] demonstrated that electrically inactive implantation-induced defects can exist up to 700 °C.

After a gradual recovery up to temperatures of 200 to 300 °C, depending on the ion mass and ascribed to decreasing local compensation as discussed below, the VO signal starts to disappear at ~350 °C (Fig. 4). The main annihilation mechanisms of VO are anticipated to be (i) migration and trapping by O_i atoms yielding VO_2 pairs which are predominantly electrically neutral and (ii) dissociation ($VO \rightarrow V+O_i$).[11,37,38]

At and above ~300 °C, also the diffusion length of V_2 is sufficient to promote reactions with O_i atoms in our samples

(concentration of $O_i \sim 10^{16}-10^{17}$ cm^{-3}) and the V_2O pair emerges (Fig. 4). These pairs are expected to have a similar or wider spatial distribution away from the initial ion trajectory compared to that of VO and should be less influenced by the local compensation than the VO (and V_2) centers. Thus, the difference in amplitude between the $V_2O(=/-)$ and $V_2O(-/0)$ peaks may possibly be used as an indication of the strength of the local compensation. Unfortunately, an additional level overlapping with the $V_2(-/0)$ and $V_2O(-/0)$ levels arises in the similar temperature interval as V_2O emerges, as discussed in Refs. 16, 29, and 30. The strength of this overlapping level amounts to ~15% of the initial V_2 concentration, but the identity of the level is not known. The overlap is mainly with the $V_2O(-/0)$ level rather than with $V_2(-/0)$; in fact, even using DLTS weighting functions with high-energy resolution, such as GS4 and GS6,[39] or Laplace-DLTS, it has not been possible to distinguish between the different contributions with a high degree of accuracy because of a too-low signal-to-noise ratio. However, assuming that the amplitude of the $V_2O(-/0)$ peak has a one-to-one correlation with that of $V_2O(=/-)$, i.e., V_2O is not affected by local compensation, the thermal evolution of the overlapping level can be deduced, as shown in Fig. 11. Interestingly, as revealed by Fig. 11(b) the thermal evolution of the relative amplitude of the overlapping level is almost identical for all the different ions, with a possible exception for He, and also very similar to that observed in electron-irradiated samples.[16,30] Hence, these results may be regarded as supporting evidence for the assumption that the V_2O centers are not affected by local compensation and dilute conditions prevail after annealing above ~300°. However, further work is required to unambiguously confirm this conclusion.

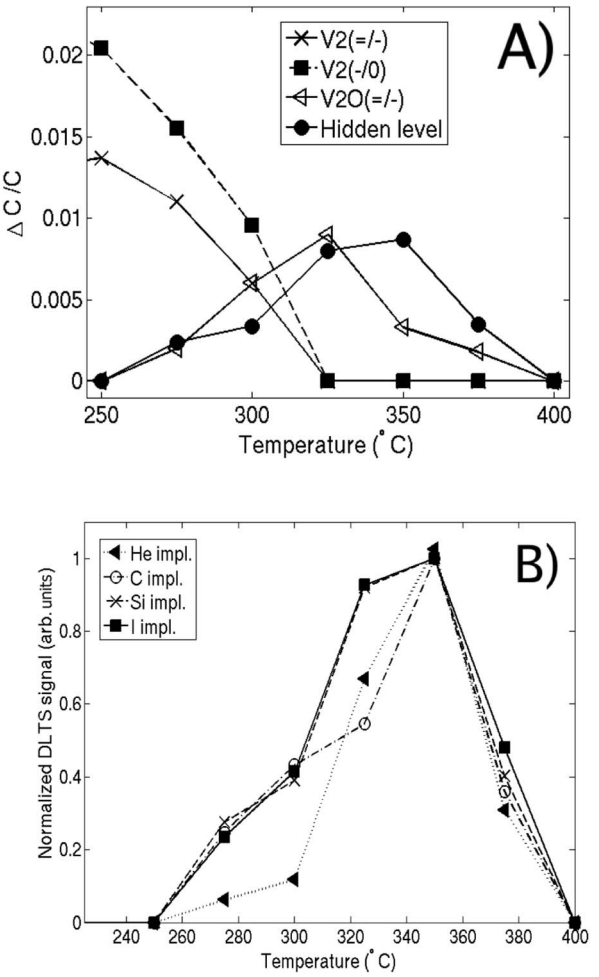

FIG. 11. (a) Defect evolution during isochronal annealing of Si implanted samples where the amplitude of the level overlapping with the $V_2O(-/0)$ peak is estimated by assuming that the contribution of the $V_2O(-/0)$ signal is equal to that of the $V_2O(=/-)$ peak and (b) normalized amplitude of the overlapping level versus annealing temperature for the He, C, Si, and I-implanted samples. The normalization is performed with respect to the peak amplitude value extracted at 350 °C.

V. CONCLUSIONS

He, C, Si, and I ions, with energies from 2.75 to 46 MeV and doses from 10^6 to 10^9 cm^{-2}, have been implanted in impurity-lean epitaxially grown *n*-type silicon at RT and the samples were subsequently analyzed by DLTS. The levels originating from the VO center and the doubly negative charge state of V_2 decrease in concentration relative to that of the singly negative charge state of V_2 with increasing ion mass. Concurrently, all the three levels (VO, $V_2(=/-)$, and $V_2(-/0)$) exhibit a reduction in the capture rate of electrons as the ion mass is increased, and unambiguous evidence is obtained for local carrier compensation in defect-rich regions. Annealing at temperatures above ~150 °C reveal a gradual decrease in the $V_2(-/0)$ peak, accompanied by a growth of both the VO and $V_2(=/-)$ peaks as well as a recovery of the electron capture rates for all the three levels. In order to account for these experimental observations, an interpretation is put forward which hinges closely on the strong localization of the defect generation by single-ion impacts and Fermi-level pinning by the $V_2(-/0)$ state. Especially, based on TCAD simulations of the electron occupancy of the defect states and Monte Carlo simulations of the spatial defect distributions, the experimentally observed deviation from a one-to-one proportionality between the amplitudes of the $V_2(=/-)$ and $V_2(-/0)$ peaks is quantitatively modeled with good accuracy. The model distinguishes between V_2 centers located in regions with a high defect density, V_2^{dense}, and with a low defect density, V_2^{dilute}. Both V_2^{dense} and V_2^{dilute} contribute to the $V_2(-/0)$ peak while the $V_2(=/-)$ peak is determined by V_2^{dilute} only since the carrier compensation in the defect-rich regions prevents filling of the doubly negative charge state of V_2^{dense}. Irrespective of the ion mass used, the regions with V_2^{dense} and V_2^{dilute} can be distinguished by a threshold for the defect generation rate having a constant value (1.2 vacancies/ion/Å), which is a support for the validity of the model. Finally, annealing at temperatures $\gtrsim$300 °C reduces the strong localization of the spatial defect distributions, as shown by migration of V_2 and subsequent trapping by O_i atoms to form V_2O pairs.

ACKNOWLEDGMENT

This work was supported by the Norwegian Research Council through the NanoMat program.

*lasse.vines@fys.uio.no

[1] G. Bemski, J. Appl. Phys. **30**, 1195 (1959).
[2] J. W. Corbett and G. D. Watkins, Phys. Rev. Lett. **7**, 314 (1961).
[3] G. D. Watkins and J. W. Corbett, Phys. Rev. **138**, A543 (1965).
[4] A. Hallén, B. U. R. Sundquist, Z. Paska, B. G. Svensson, M. Rosling, and J. Tirén, J. Appl. Phys. **67**, 1266 (1990).
[5] B. G. Svensson, B. Mohadjeri, A. Hallén, J. H. Svensson, and J. W. Corbett, Phys. Rev. B **43**, 2292 (1991).
[6] A. O. Evwaraye and E. Sun, J. Appl. Phys. **47**, 3776 (1976).
[7] B. G. Svensson and M. Willander, J. Appl. Phys. **62**, 2758 (1987).
[8] B. G. Svensson, C. Jagadish, A. Hallén, and J. Lalita, Phys. Rev. B **55**, 10498 (1997).
[9] R. M. Fleming, C. H. Seager, D. V. Lang, E. Bielejec, and J. M. Campbell, Appl. Phys. Lett. **90**, 172105 (2007).
[10] R. M. Fleming, C. H. Seager, D. V. Lang, P. J. Cooper, E. Bielejec, and J. M. Campbell, J. Appl. Phys. **102**, 043711 (2007).
[11] P. Pellegrino, P. Lévêque, J. Lalita, A. Hallén, C. Jagadish, and B. G. Svensson, Phys. Rev. B **64**, 195211 (2001).
[12] E. V. Monakhov, J. Wong-Leung, A. Yu. Kuznetsov, C. Jagadish, and B. G. Svensson, Phys. Rev. B **65**, 245201 (2002).
[13] N. Abdelgader and J. H. Evans-Freeman, J. Appl. Phys. **93**, 5118 (2003).
[14] N. Keskitalo, A. Hallén, J. Lalita, and B. G. Svensson, in *Defects and Diffusion in Silicon Processing*, edited by S. Coffa *et al.*, MRS Symposia Proceedings No. 469 (Materials Research Society, Pittsburgh, 1997), p. 233.
[15] L. Vines, E. V. Monakhov, B. G. Svensson, J. Jensen, A. Hallén, and A. Yu. Kuznetsov, Phys. Rev. B **73**, 085312 (2006).
[16] M. Mikelsen, E. V. Monakhov, G. Alfieri, B. S. Avset, and B. G. Svensson, Phys. Rev. B **72**, 195207 (2005).
[17] E. V. Monakhov, B. S. Avset, A. Hallén, and B. G. Svensson, Phys. Rev. B **65**, 233207 (2002).
[18] A. Kawasuso, M. Hasegawa, M. Suezawa, S. Yamaguchi, and K. Sumino, Appl. Surf. Sci. **85**, 280 (1995).
[19] V. P. Markevich, A. R. Peaker, S. B. Lastovskii, L. I. Murin, and J. L. Lindström, J. Phys.: Condens. Matter **15**, S2779 (2003).
[20] B. G. Svensson, K.-H. Rydén, and B. M. S. Lewerentz, J. Appl. Phys. **66**, 1699 (1989).
[21] J. F. Ziegler, J. P. Biersack, and U. Littmark, *The Stopping and Range of Ions in Solids* (Pergamon, New York, 1985).
[22] Synopsys Inc., 700 East Middlefield Road, Mountain View, CA 94043, USA (see also http://www.synopsys.com/).
[23] A. Hallén, N. Keskitalo, F. Masszi, and V. Nágl, J. Appl. Phys. **79**, 3906 (1996).
[24] B. G. Svensson and J. L. Lindström, J. Appl. Phys. **72**, 5616 (1992).
[25] T. Diaz de la Rubia and G. H. Gilmer, Phys. Rev. Lett. **74**, 2507 (1995).
[26] M. J. Caturla, T. Díaz de la Rubia, L. A. Marqúes, and G. H. Gilmer, Phys. Rev. B **54**, 16683 (1996).
[27] K. Nordlund, M. Ghaly, R. S. Averback, M. Caturla, T. Diaz de la Rubia, and J. Tarus, Phys. Rev. B **57**, 7556 (1998).
[28] S. D. Brotherton and P. Bradley, J. Appl. Phys. **53**, 5720 (1982).
[29] M. Mikelsen, E. V. Monakhov, G. Alfieri, B. S. Avset, J. Härkönen, and B. G. Svensson, J. Phys.: Condens. Matter **17**, S2247 (2005).
[30] L. S. Løvlie, MA thesis, University of Oslo, 2007.
[31] W. Jung and G. S. Newell, Phys. Rev. **132**, 648 (1963).
[32] M. Nisenoff and H. Y. Fan, Phys. Rev. **128**, 1605 (1962).
[33] Y. H. Lee and J. W. Corbett, Phys. Rev. B **8**, 2810 (1973).
[34] T. E. M. Staab, A. Sieck, M. Haugk, M. J. Puska, T. Frauenheim, and H. S. Leipner, Phys. Rev. B **65**, 115210 (2002).
[35] S. K. Estreicher, J. L. Hastings, and P. A. Fedders, Appl. Phys. Lett. **70**, 432 (1997).
[36] B. Holm and K. Bonde Nielsen, J. Appl. Phys. **78**, 5970 (1995).
[37] B. G. Svensson and J. L. Lindström, Phys. Rev. B **34**, 8709 (1986).
[38] M. Mikelsen, J. H. Bleka, J. S. Christensen, E. V. Monakhov, B. G. Svensson, J. Härkönen, and B. S. Avset, Phys. Rev. B **75**, 155202 (2007).
[39] A. A. Istratov, J. Appl. Phys. **82**, 2965 (1997).